論文 / 著書情報
Article / Book Information

Title	Experimental measurement of moisture distribution in the adhesive layer using near-infrared spectroscopy
Authors	Jin-Woo Han, Yu Sekiguchi, Kazumasa Shimamoto, Haruhisa Akiyama, Chiaki Sato
Citation	Journal of Applied Polymer Science, Vol. 140, Issue 25, e53982
Pub. date	2023, 4
DOI	https://doi.org/10.1002/app.53982
Creative Commons	Information is in the article.

Received: 21 February 2023 | Revised: 6 April 2023 | Accepted: 8 April 2023

DOI: 10.1002/app.53982

RESEARCH ARTICLE

Applied Polymer SCIENCE WILEY

Experimental measurement of moisture distribution in the adhesive layer using near-infrared spectroscopy

Jin-Woo Han[1] | **Yu Sekiguchi**[2] | **Kazumasa Shimamoto**[3] | **Haruhisa Akiyama**[3] | **Chiaki Sato**[2]

[1]Department of Mechanical Engineering, Tokyo Institute of Technology, Yokohama, Japan

[2]Institute of Innovative Research, Tokyo Institute of Technology, Yokohama, Japan

[3]Nanomaterials Research Institute, National Institute of Advanced Industrial Science and Technology (AIST), Ibaraki, Japan

Correspondence
Jin-Woo Han, Department of Mechanical Engineering, Tokyo Institute of Technology, 4259 Nagatsuta-cho, Midori-ku, Yokohama, Kanagawa 226-8503, Japan.
Email: han.j.aj@m.titech.ac.jp

Yu Sekiguchi, Institute of Innovative Research, Tokyo Institute of Technology, 4259 Nagatsuta-cho, Midori-ku, Yokohama, Kanagawa 226-8503, Japan.
Email: sekiguchi.y.aa@m.titech.ac.jp

Funding information
New Energy and Industrial Technology Development Organization, Grant/Award Number: JPNP14014

Abstract

Adhesive joints are degraded when exposed to moist conditions, making it essential to assess the permeation distance of absorbed moisture. However, monitoring the water penetration in the adhesive layer is challenging because the adhesive layer is sandwiched between the adherends. To overcome this difficulty, we proposed a new monitoring system using fiber-type near-infrared spectroscopy (NIRS), and the moisture distribution at the joint was successfully observed by introducing quartz glass as one side of the substrate. First, the change in the absorbance spectra owing to water absorption by an epoxy adhesive was investigated by immersing epoxy-coated aluminum alloy plates in temperature-controlled water. It was found that the water content can be evaluated by monitoring the change in the peak intensity appearing around 1900–1950 nm. Next, water penetration into the adhesive layer sandwiched between the quartz glass and aluminum alloy was investigated by scanning the surface. The water permeation distance was found to change with temperature. Under the 23°C immersion condition, approximately 2.5 mm of water penetration was observed after 8 weeks. Because the simulation results using Fick's law of diffusion showed similar trends, it was experimentally confirmed that Fickian diffusion dominates the water distribution in the adhesive layer.

KEYWORDS

epoxy adhesive, hydrothermal degradation, in-situ monitoring, moisture absorption, non-destructive testing

1 | INTRODUCTION

Adhesive bonding technology has the ability to bond dissimilar materials and is therefore commonly used in manufacturing, especially in the aerospace and automobile industries.[1,2] Adhesive joints used in these applications typically experience severe loading, such as cyclic and impact loading,[3,4] and are exposed to harsh environments such as high temperature and humidity.[5] The combination of temperature, moisture, and fatigue not only accelerates the fracture of adhesively bonded joints but also makes it difficult to predict.[6] Additionally, the life of the adhesive joint in a harsh environment is extremely short because adhesives are composed of polymers that are prone to

degradation. Therefore, the durability of the joints must be carefully considered.

Under highly humid or wet conditions, the mechanical properties of the adhesive joints decrease with increasing moisture content.[7–10] It is believed that water accumulates near the interface after absorption by the adhesive layer.[11] Indeed, studies have shown that the interface strength decreases after immersion in water.[12–14] Therefore, it is important to introduce in-situ monitoring techniques for damage inspection of adhesively bonded joints due to moisture. Recently, several in-situ monitoring techniques, such as fiber optic monitoring, X-ray microtomography, digital image correlation, acoustic emissions, and mechanoluminescence, have been introduced to observe crack propagation in adhesive joints.[15–19] However, until now, there are almost no methods for direct measurement of water penetration in the adhesive layer. Degradation due to water absorption is therefore only speculative and in-situ monitoring of moisture distribution is essential to discuss what is happening.

The gravimetric method, which quantifies the total water absorption based on the initial mass and the mass after immersion, is commonly used to determine the water diffusion coefficient of a material. However, in the case of adhesive joints, the adhesive layer is sandwiched between the adherends, and only the side surfaces come into contact with moisture, resulting in a water absorption distribution in the adhesive layer. Therefore, it is important to determine the penetration distance of the absorbed moisture from the edge to assess the decrease in the bonding strength.[11,20] In numerical analysis, the water absorption distribution of the adhesive layer is calculated using material diffusion analysis based on Fick's law of diffusion.[21–23] Furthermore, the strength and toughness are calculated by inputting the changes in the physical property according to the amount of moisture absorption.[12,24–33] In some studies, the amount of water absorption has been experimentally investigated by monitoring the changes in the strain,[22,34] which are induced by the swelling associated with moisture absorption, and changes in the modulus,[35] or by using electrochemical impedance spectroscopy.[36] Fourier-transform infrared (FTIR)-transmission microscopy has been used to measure the diffusion of D_2O in the adhesive layer,[37,38]

TABLE 1 Chemical composition of the adhesive used in this study.

Material	Mass (%)
Bisphenol A epoxy resin	24
Carboxyl-terminated butadiene acrylonitrile rubber Modified epoxy resin (elastomer 40%)	39
Fumed silica	3
Filler ($CaCO_3$)	26
CaO	2
Dicyandiamide	5
3-(3,4-dichlorophenyl)-1,1′-dimethylurea	1

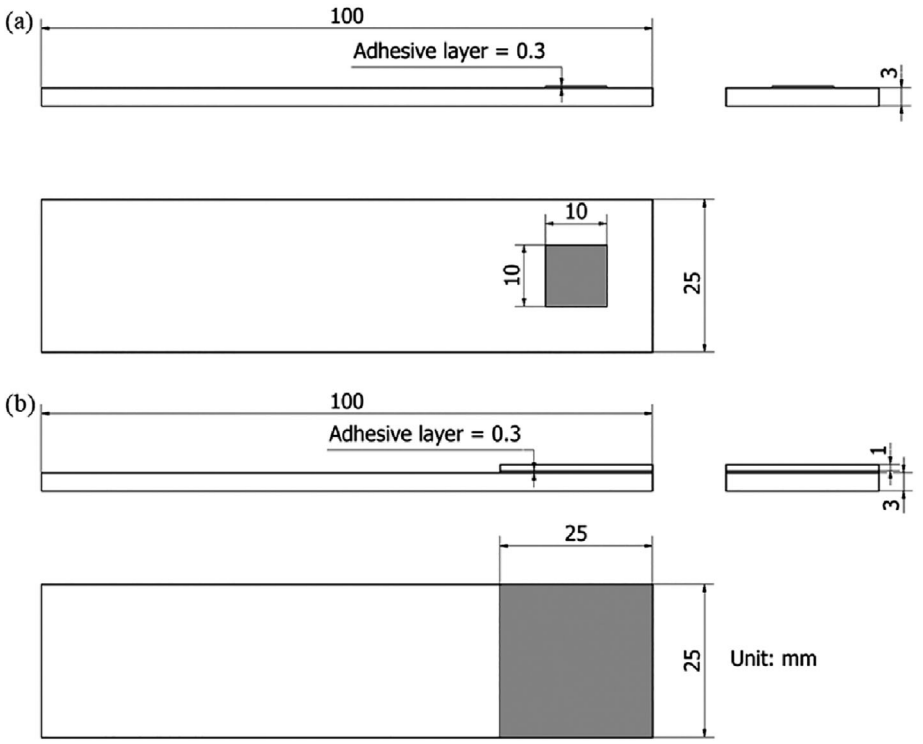

FIGURE 1 Schematic of the (a) open-faced specimen and (b) closed specimen.

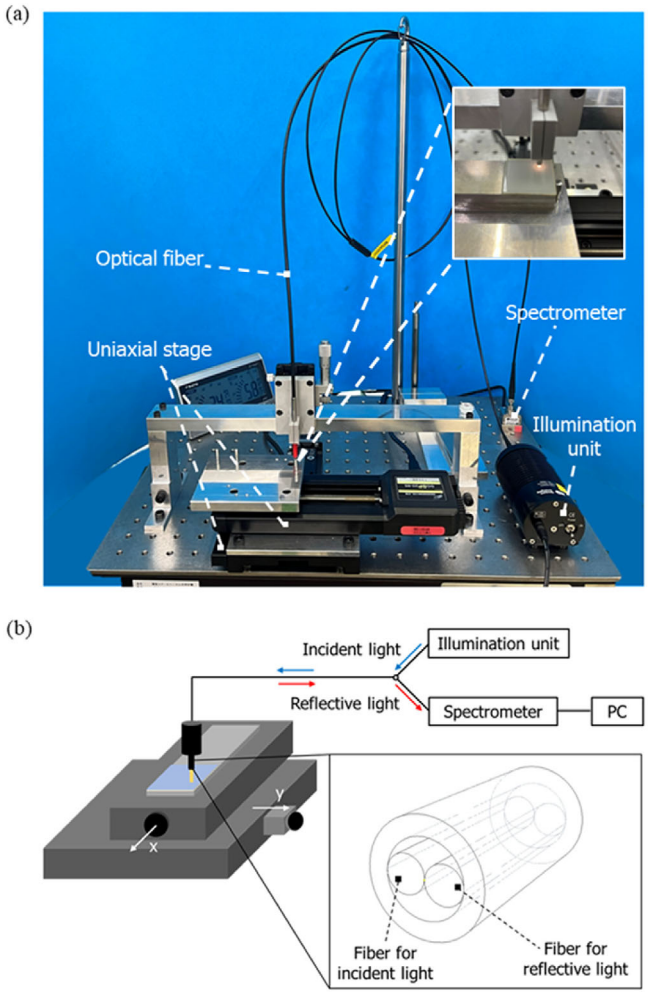

FIGURE 2 (a) Photograph of the NIRS setup and (b) schematic of the operation of the instrument. [Color figure can be viewed at wileyonlinelibrary.com]

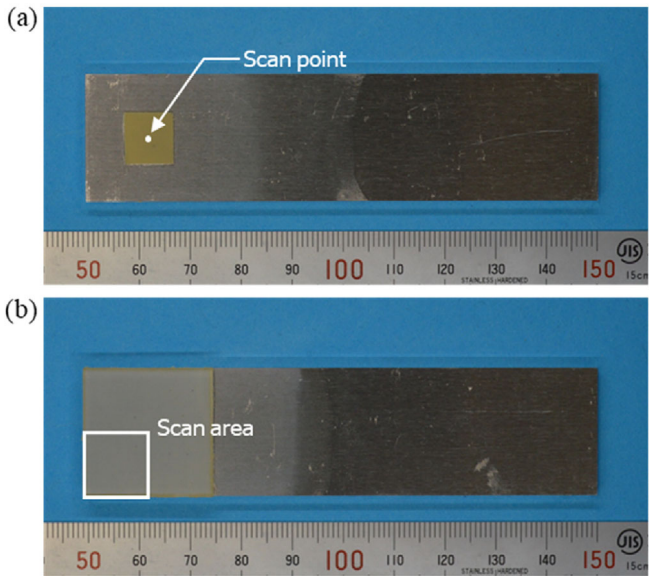

FIGURE 3 Scanning area of (a) open-faced specimen and (b) closed specimen. [Color figure can be viewed at wileyonlinelibrary.com]

but there are very few experimental examples of non-destructive observations of water distribution in the adhesive layer. Therefore, non-destructive testing (NDT) methods for in-situ observation of water penetration need to be developed.

Non-destructive testing is a technique for inspecting an object without destroying it; this inspection method has been adopted in many industries because it allows the object to be used immediately after inspection. Ultrasound, x-ray, radiation, infrared, or acoustic emission waves are used for defect detection and thickness measurement. In the case of adhesive joints, defects, such as voids and weak bonds, can be detected using ultrasonic NDT.[39,40] Near-infrared spectroscopy (NIRS) is widely used to measure the moisture content in fields, such as pharmaceuticals,[41] foods,[42,43] and polymers.[44,45] This is because a major absorption band of H_2O exists in the NIR wavelength range. Spatial analysis of NIRS has also been conducted using hyperspectral imaging (HSI),[46,47] and successful visualization of the residual moisture content has been reported.[48] However, because complex spectral image analysis is typically required, an image-processing technique using deep learning has been proposed.[49] Furthermore, owing to the instrumental limitations of hyperspectral cameras, high-resolution scanning remains challenging. Therefore, a method was developed to construct a hyperspectral image with much higher spatial resolution from multiple low-resolution hyperspectral images.[50] Thus, even with HSI, the determination of moisture content is not straightforward. In contrast, the miniaturization of NIRS sensors has been remarkable, and various applications have been reported.[51] The equipment and measurement technology of NIRS are continuously evolving, revealing immense possibilities.

The spatial resolution, data analysis, and measurement methods are particularly important when considering the application of NIRS for monitoring the changes in the moisture distribution in the adhesive layer. Metals are one of the major substrate materials that are bonded with adhesives. However, NIR rays cannot penetrate metals and so this technology cannot be used to analyze the adhesive layers sandwiched between metal plates. In other words, if a material that can transmit NIR rays is selected for the substrate, it may be possible to measure the absorption of water. When scanning adhesively bonded plastics, the NIR rays can reach the adhesive layer, but the moisture absorbed by the adherends is also detected. Therefore, it is impractical to use plastics as adherends. In contrast, if glass plates are used as the

adherends, these problems can be avoided and the water absorption of the adhesive layer can be detected. Due to its high transmittance in the wavelength range up to 2600 nm, quartz glass plate is commonly used in NIRS.[52,53] When one side of the substrate is a quartz glass plate and the other side is a metal plate, the NIR rays

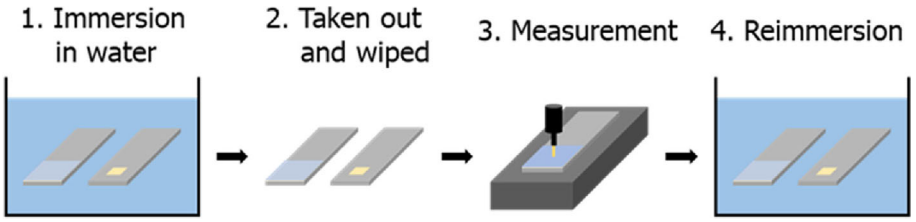

FIGURE 4 Schematic of the immersion and measurement procedure. [Color figure can be viewed at wileyonlinelibrary.com]

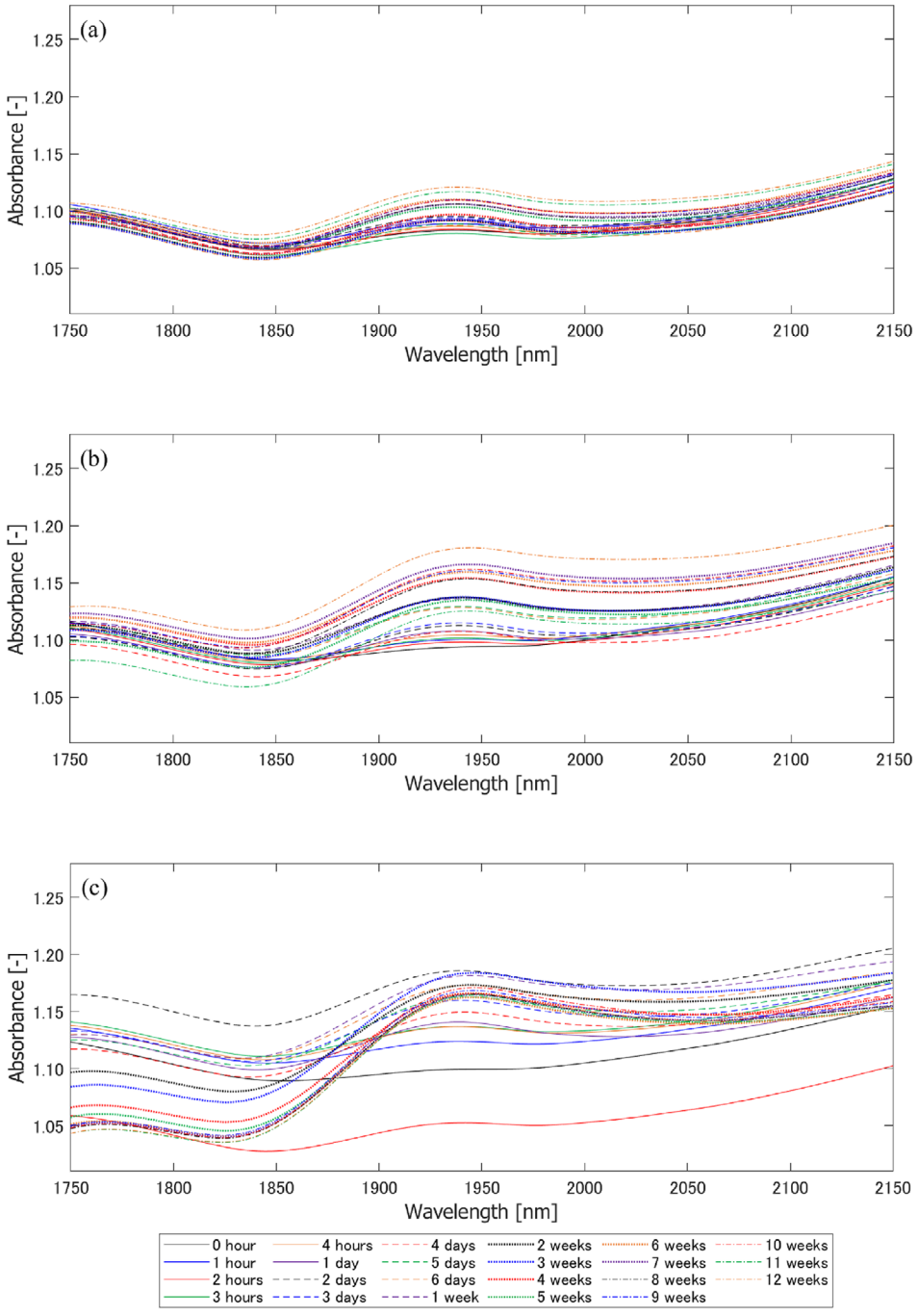

FIGURE 5 Absorbance spectra of the open-faced specimens at (a) 23°C, (b) 42°C, and (c) 63°C from 0 h (before immersion) unit 12 weeks. [Color figure can be viewed at wileyonlinelibrary.com]

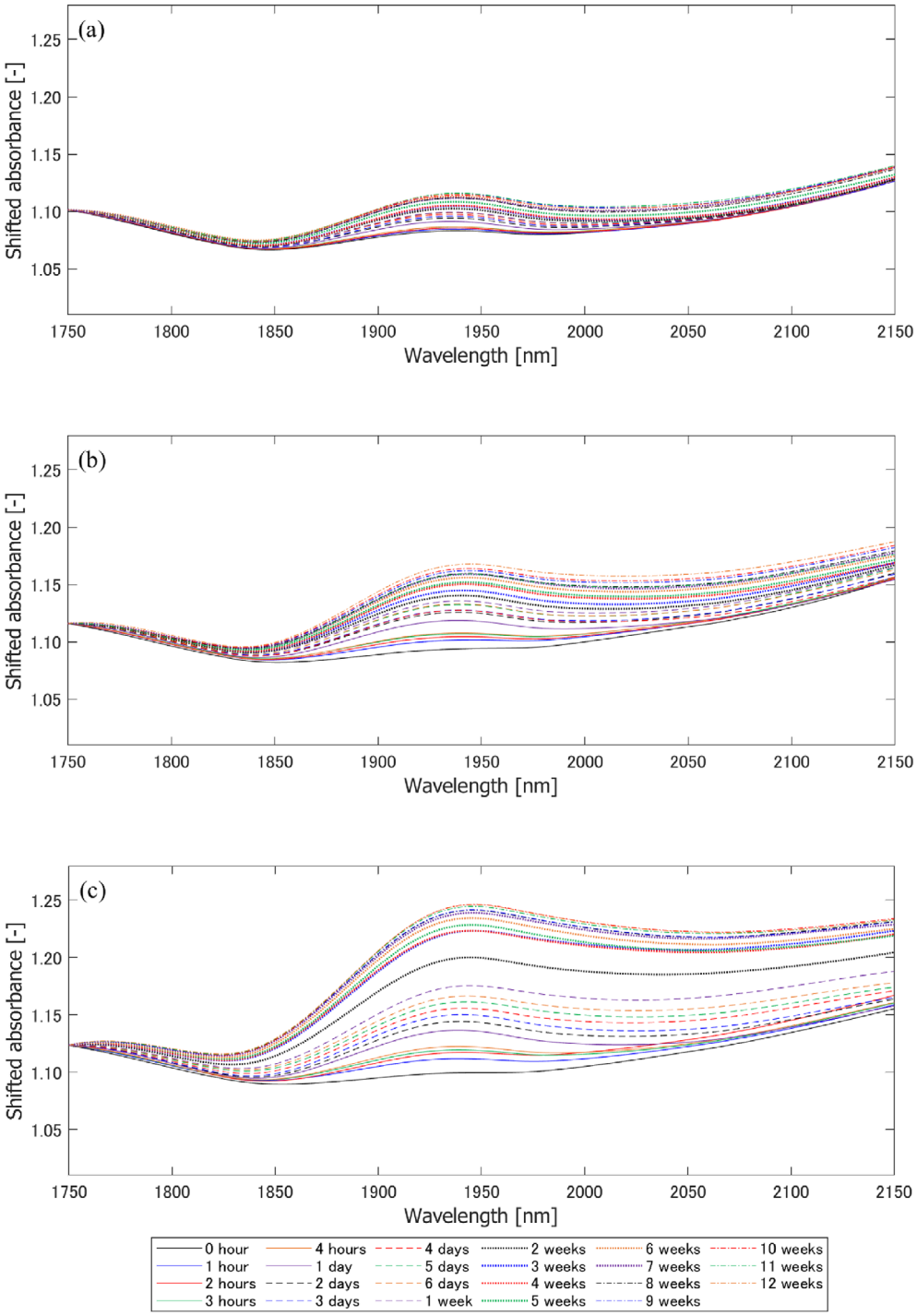

FIGURE 6 Absorbance spectra of the open-faced specimens shifted to match 1750 nm values at (a) 23°C, (b) 42°C, and (c) 63°C from 0 h (before immersion) unit 12 weeks. [Color figure can be viewed at wileyonlinelibrary.com]

pass through the adhesive layer, are reflected at the interface between the adhesive and metal, and pass through the adhesive layer again. Because specific wavelengths of light are selectively absorbed by the adhesive layer, the absorbance spectrum contains information about the chemical composition of the adhesive layer.

In this study, a fiber-type NIRS instrument and an automatic XY-axis stage were installed to scan the moisture contained in the epoxy adhesive. First, the spectrum change due to the moisture absorption of the epoxy material was investigated, focusing on the peak intensity at approximately 1900–1950 nm. The obtained spectrum was processed using Python code specialized for NIRS analysis. Next, the moisture absorption diffusion according to the immersion temperature and time was investigated by surface scanning of the adhesive layer between an aluminum alloy plate and a quartz glass plate, and the obtained results were compared with the numerical results.

2 | EXPERIMENTAL

2.1 | Materials and specimens

A thermoset epoxy adhesive, supplied by Cemedine Co., Ltd. (Tokyo, Japan), was used in this study; the composition of the adhesive is shown in Table 1. It is one of the traditional structural epoxy adhesives with bisphenol A epoxy as a base resin and dicyandiamide (DICY) as a curing agent. By containing carboxyl-terminated butadiene acrylonitrile (CTBN) rubber, a good balance of strength and toughness was achieved. Considering the

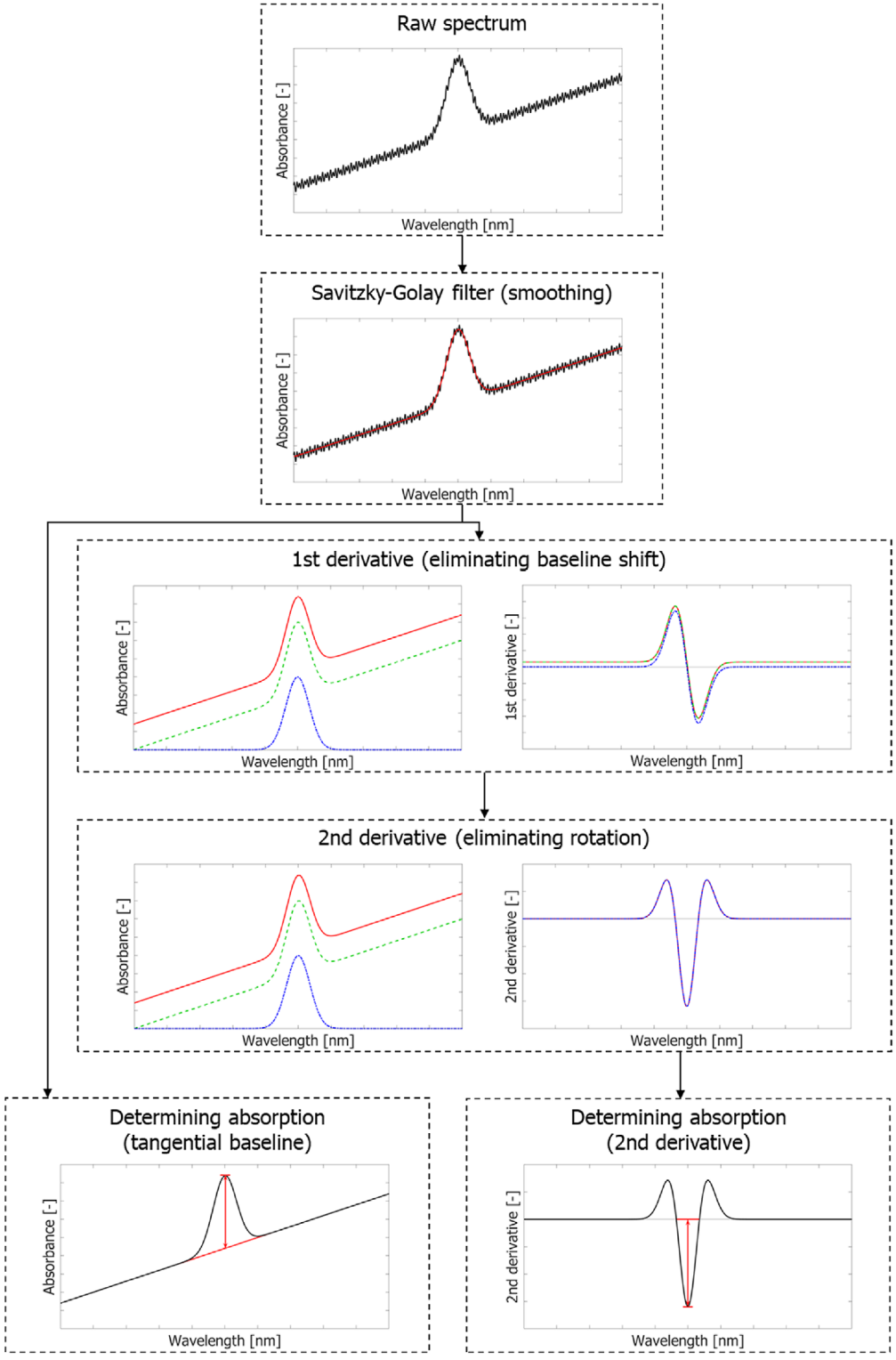

FIGURE 7 Flowchart of data processing for calculating peak intensity. [Color figure can be viewed at wileyonlinelibrary.com]

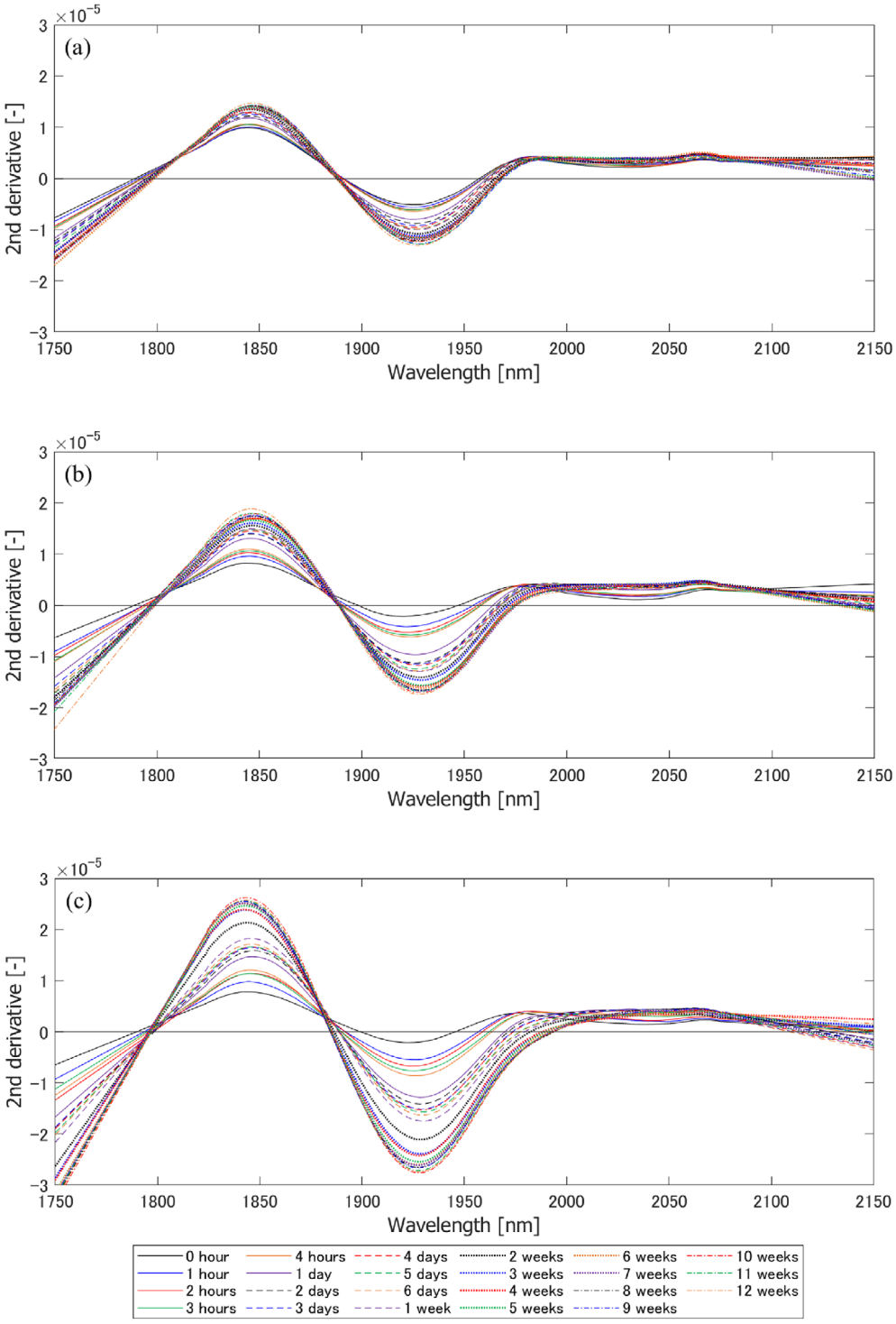

FIGURE 8 Second derivative spectra of the open-faced specimens at (a) 23°C; (b) 42°C; (c) 63°C from 0 h (before immersion) unit 12 weeks. [Color figure can be viewed at wileyonlinelibrary.com]

temperature and time required for sufficient completion of the adhesive curing reaction, curing was conducted at 180°C for 60 min.

Two types of specimens were prepared. The open-faced specimens were prepared by applying only the epoxy adhesive with a thickness of 0.3 mm on the aluminum alloy substrate. The adhesive application area was 100 mm^2 as shown in Figure 1a. The thickness was adjusted by attaching polytetrafluoroethylene tape with a thickness of 0.3 mm to the four sides. This adhesive layer was similar to a coating, resulting in uniform and fast moisture absorption. Therefore, they were used for analyzing the spectral change due to water absorption in the epoxy. The closed specimens were prepared by bonding the aluminum alloy substrate and the quartz glass plate. The entire surface of the glass plate was adhered to the aluminum alloy plate, that is, the adhesive application area was 625 mm^2, as shown in Figure 1b. Glass beads of

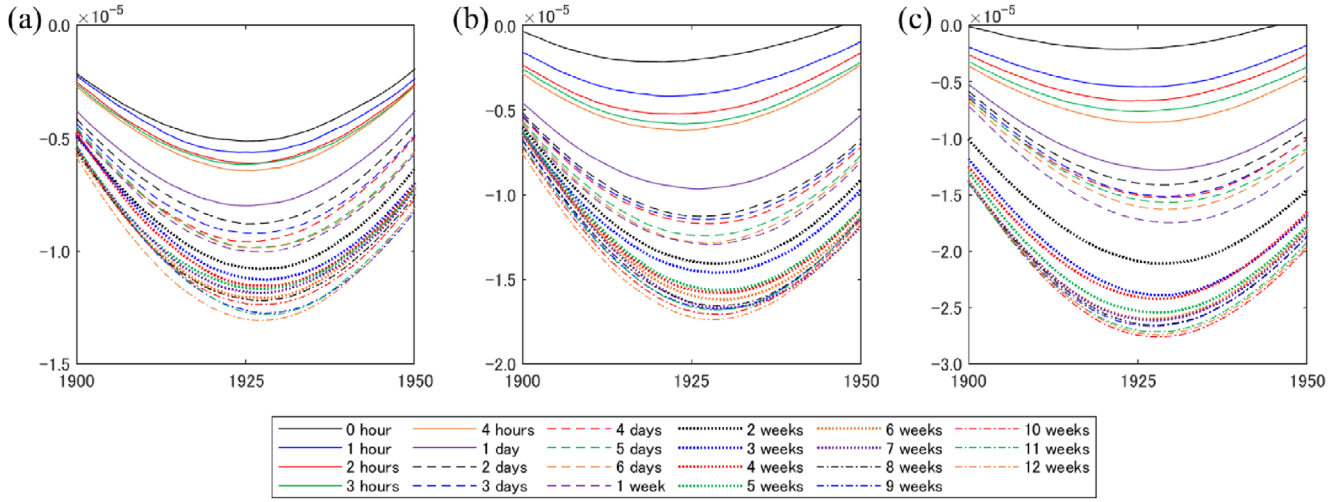

FIGURE 9 Magnified view of second derivative spectra in a wavelength range of 1890–1990 nm at (a) 23°C, (b) 42°C, and (c) 63°C. [Color figure can be viewed at wileyonlinelibrary.com]

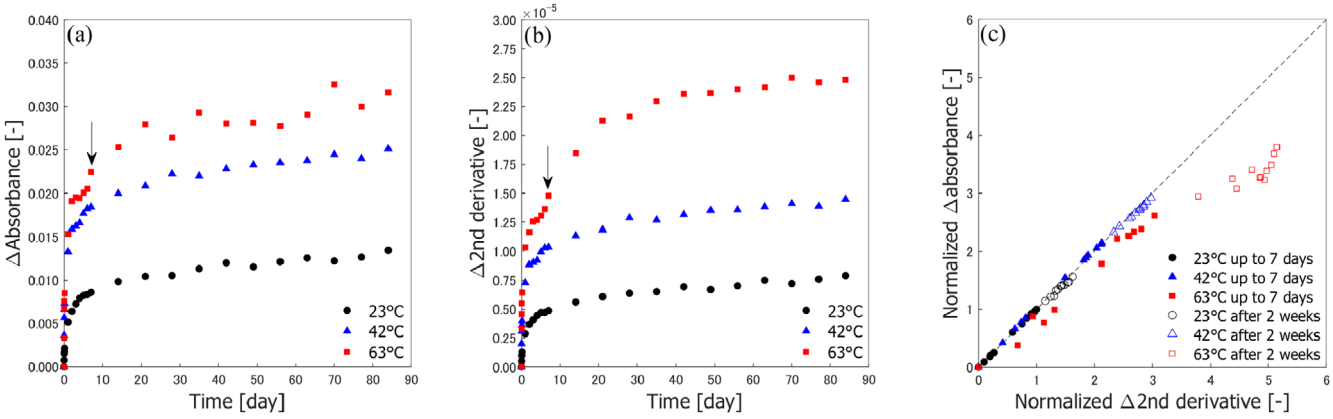

FIGURE 10 Peak intensity increments of (a) absorbance spectra and (b) second derivative spectra, and (c) comparison of both methods. The specimens used for the measurement are an open-faced specimen, with immersion temperatures of 23°C, 42°C, and 63°C. [Color figure can be viewed at wileyonlinelibrary.com]

0.3 mm diameter were inserted to control the thickness of the adhesive layer. Because water penetrated only from the surroundings, these specimens were used to analyze the moisture distribution in the adhesive layer.

A6061-T6 aluminum alloy plate with a thickness of 3 mm, width of 25 mm, and length of 100 mm was used as the bottom substrate for both types of specimens. The aluminum alloy was first degreased with acetone. Subsequently, it was immersed in an alkaline solution at 60°C for 30 s, followed by washing with purified water and drying. Afterward, it was immersed in an acidic solution at 60°C for 30 s. A synthetic quartz glass plate with a thickness of 1 mm and width/length of 25 mm was used as the top substrate of the closed specimens. The surface of the glass plate was degreased with acetone prior to bonding.

2.2 | Measurement system

The setup of the NIR measurement system is shown in Figure 2a. The main components of the system included an NIR spectrometer (NIRONE S2.2, Spectral Engines, Steinbach, Germany), an illumination unit consisting of a tungsten halogen lamp (HL-2000-LL, Ocean Insight, Orland, USA), an automatic two-axis stage operated by stepping motors (SGSP20-85 for the x-axis and HPS120-60X for the y-axis, Sigma Koki Co., Tokyo, Japan), and a bifurcated optical fiber bundle.

Figure 2b shows the schematic of the operation of the instrument. The light from the illumination unit irradiated the specimen along the optical fiber; the reflected light entered the optical fiber again and was measured with a spectrometer based on a Fabry–Pérot interferometer.

The spectral data were scanned over the range of 1750–2150 nm at a point with a wavelength interval of 1 nm for the open-faced specimens and in a plane with a wavelength interval of 5 nm for the closed specimens. All scans were performed under laboratory conditions. The scanning area for each type of specimen is shown in Figure 3. In the case of the closed specimens, it took approximately 1 s to scan from 1750 to 2150 nm and move to the next point. The scanning pitch was set to 0.5 mm, and a total of 625 points were scanned. Therefore, the scan time was approximately 11 min for each surface scan.

2.3 | Immersion conditions

The temperature of purified water for immersion was set to room temperature (approximately 23°C), 42°C, and 63°C according to our previous study using the same adhesive.[13] In the case of 23°C immersion, the specimens were placed in a plastic bag with the purified water. In the case of 42 and 63°C immersion, the specimens were placed in a plastic bag with the purified water and the plastic bag was placed in a temperature-controlled water bath. Scanning was initially performed hourly, every 24 h after 4 h, and then weekly after 1 week. The scanning procedure is illustrated in Figure 4. The specimen was removed from the water bath for scanning. After wiping the surface, the specimen was scanned and re-immersed in the water bath. The scanning time was not included in the immersion time.

2.4 | Spectroscopic analysis

The reflectance spectra were converted to absorbance values calculated as $-\log_{10}(I/I_0)$, where I is the measured intensity and I_0 is the background intensity. A background spectrum was obtained prior to each test by using test specimens in which the adhesive layer was replaced by an air gap of the same thickness between the glass and aluminum alloy plates. For NIRS data analysis, spectral preprocessing techniques are required to remove irrelevant information, including noise, uncertainties, variability, and interactions.[54] An open-source preprocessing module nippy, created in Python 3.10,[55] was introduced to acquire the preprocessed spectra. A smoothing process (Savitzky–Golay filter with a 3rd order polynomial) and derivative process (second derivative with filter windows of 150 for open-faced specimens and 15 for closed specimens) were used for the evaluation.

Two methods were introduced to calculate the moisture absorption level in this study. The first method involved calculating the peak intensities of the absorbance spectra. However, changes in the absorbance spectra include various influences other than moisture, and even if the peak value is used as is, the correct amount of water absorption cannot be expressed. Therefore, a tangential baseline correction was applied. A straight baseline was drawn between the two valleys of the absorbance spectrum, and the distance from the peak to the baseline was considered the intensity of absorption.[56] The second method involves calculating the peak intensities of the second derivative spectra. In quantitative analysis, the second derivative technique has the advantage of improving the accuracy of quantification by eliminating the baseline shift in the spectra.[57] The peak of the absorbance spectrum corresponds to the negative peak of the second derivative spectrum; therefore, the absolute value of the second derivative peak has a linear relationship with the amount

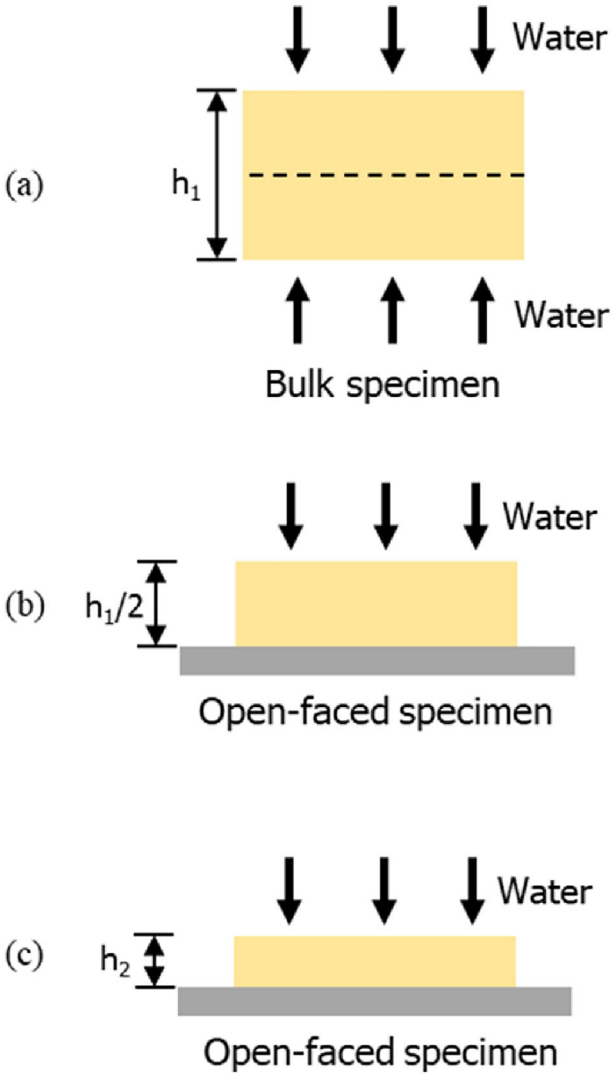

FIGURE 11 The difference in water containment speed with different thicknesses and different types in specimens. (a) Bulk specimen with thickness of h_1, (b) open-faced specimen with thickness of $h_1/2$, and (c) open-faced specimen with thickness of h_2. [Color figure can be viewed at wileyonlinelibrary.com]

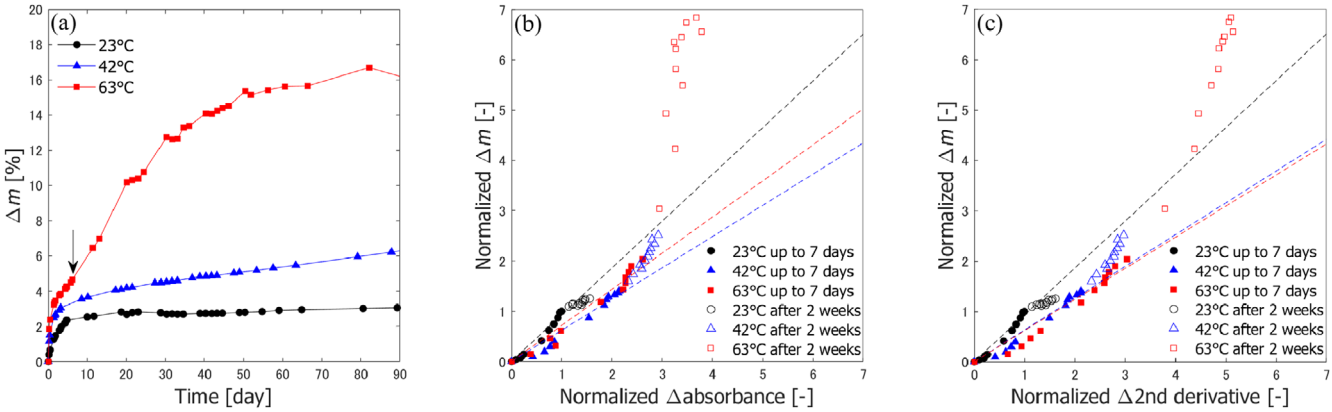

FIGURE 12 (a) Weight increments of bulk specimens and their variation against peak intensities of (b) absorbance spectra and (c) second derivative spectra with immersion temperatures of 23°C, 42°C, and 63°C. [Color figure can be viewed at wileyonlinelibrary.com]

Temperature	Absorbance spectrum		Second derivative spectrum	
T (°C)	k	R^2	k	R^2
23	0.930	0.962	0.930	0.959
42	0.621	0.954	0.631	0.960
63	0.718	0.958	0.618	0.946

TABLE 2 Slopes and coefficient of determination obtained by fitting $y = kx$ in the analysis of the weight increments versus peak intensities of the absorbance spectra and second derivative spectra for the data up to 7 days.

of absorption. The moisture distribution of the closed specimen was visualized by plotting the absorption of moisture determined using the two methods at each coordinate.

3 | RESULTS AND DISCUSSION

3.1 | Spectral analysis of open-faced specimens

3.1.1 | Absorbance spectrum and second derivative spectrum

The absorbance spectra of the open-faced specimens are shown in Figure 5. The absorption peak at approximately 1940 nm was caused by the O—H δ 2nd overtone.[58] However, the absorbance spectra shifted up and down with each measurement owing to several effects. Therefore, the absorbance values were shifted accordingly to match the values at 1750 nm, as shown in Figure 6, with a more pronounced increase in the peak with increasing immersion time. A counterclockwise rotation of the spectra was also observed, especially at 63°C (see Figure 6c). Therefore, the discrepancy in the values at 2150 nm increased further. The shift and rotation of the spectra might have been caused by the changes in the refractive index due to the absorbed moisture, the absorbance band with the peak outside the measurement region, and other factors.[59] Therefore, data processing is required for quantitative analysis.[57,60] The schematic flow of data processing used in this study is shown in Figure 7. After smoothing the data using the Savitzky-Golay filter, baseline is drawn for a tangential baseline correction to obtain the peak intensity of the absorbance spectrum and data are differentiated twice for a second derivative method to obtain the peak intensity of the second derivative spectrum. In the second derivative method, the linear shift effect was deleted in the first derivative, and the rotation effect in the second derivative. Therefore, red and green lines overlap for the first derivative and all lines for the second derivative graphs shown in Figure 7. The results of second derivative spectra are shown in Figures 8 and 9. The moisture peak in the second derivative spectrum appears as a negative peak at approximately 1900–1950 nm. Although linear shift and rotation effects were included in the original spectrum in Figures 5 and 6, these effects were removed from the second derivative spectrum and the change in the peak intensity with increasing immersion time can be quantitatively discussed.

3.1.2 | Determination of moisture absorption

To analyze the data quantitatively, the peak intensity of the absorbance spectrum and the peak intensity of the second derivative spectrum were calculated for each

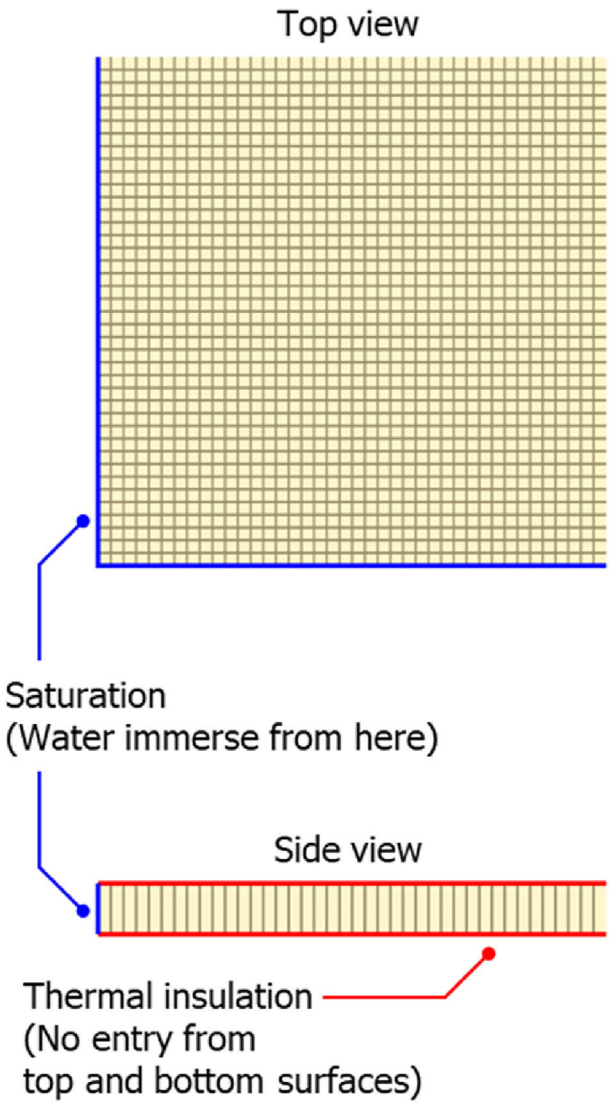

FIGURE 13 Schematic illustration of a quarter model for finite element method using heat transfer analysis. [Color figure can be viewed at wileyonlinelibrary.com]

measured time according to the data processing shown in Figure 7. The change in the intensity of the peak at approximately 1900–1950 nm over time is shown in Figure 10a for the absorbance spectrum and Figure 10b for the second derivative spectrum. The peak increment of the absorbance spectrum, that is, Δ absorbance, was defined as the change from the peak value at day 0 at each temperature. The same is true for the second derivative spectrum. The moisture absorption increased as the immersion temperature increased and tended to saturate as the immersion time increased. The increments in the intensity from the start of the test were normalized by the value at 7 days under immersion at 23°C, and the normalized values of both methods at the same time were compared, as shown in Figure 10c. The coefficients of determination for $y = x$ at 23, 42, and 63°C were 0.999, 0.989, and 0.874 for the data up to 7 days, and 0.805, 0.920, and −36.5 for the data after 2 weeks, respectively. Therefore, the linear relationship holds, except for the results at 63°C after 2 weeks.

3.1.3 | Quantitative evaluation of moisture absorption

The gravimetric method was also used for comparison with the NIRS results. Epoxy bulk specimens with a diameter of 50 mm and thickness of 0.5 mm were immersed in temperature-controlled water, and the increase in weight was measured continuously. Water penetrated from only one direction in the open-faced specimens, but from both sides in the bulk specimens. Therefore, the bulk specimens absorbed water twice as quickly. In addition, there was a difference in the thickness: 0.3 mm for the open-faced and 0.5 mm for the bulk specimens. When comparing the bulk and open-faced specimens, as shown in Figure 11a, b, the weight increment speed is the same when the thickness of the open-faced specimen is half of the bulk specimen. When comparing the open-faced specimens with different thicknesses, as shown in Figure 11b, c,

$$\left(\frac{t_2}{t_1}\right) = \left(\frac{h_2}{h_1/2}\right)^2 \quad (1)$$

is given for the same weight increment percentage, where t_1 and t_2 are the time of the open-faced specimens with the thickness $h_1/2$ and h_2, respectively. Therefore, the water absorption rate of open-faced specimens with the thickness of 0.3 mm was 1.44 times slower than that of the bulk specimens with the thickness of 0.5 mm, and the comparison of the weight increment versus time was performed after converting the absorption speed. Figure 12a shows the weight increments of the bulk specimens after the time conversion. Although the general trends are similar, a closer look reveals differences, particularly under long-term immersion. The gravimetric test results followed the Fick's law of diffusion at 23°C, but the mass continuously increased at 42 and 63°C, which was attributed to dual-stage moisture diffusion. Especially, the trend at 63°C significantly deviated from that of the intensity changes. The weight increase at 63°C after 90 days was approximately five times that at 23°C. In other words, at 63°C, the sample absorbed five times as much water as the saturated water content at 23°C. Dual-stage diffusion, which is a combination of Fickian diffusion and non-Fickian diffusion or double-Fickian diffusion, is often observed in epoxy materials.[61,62]

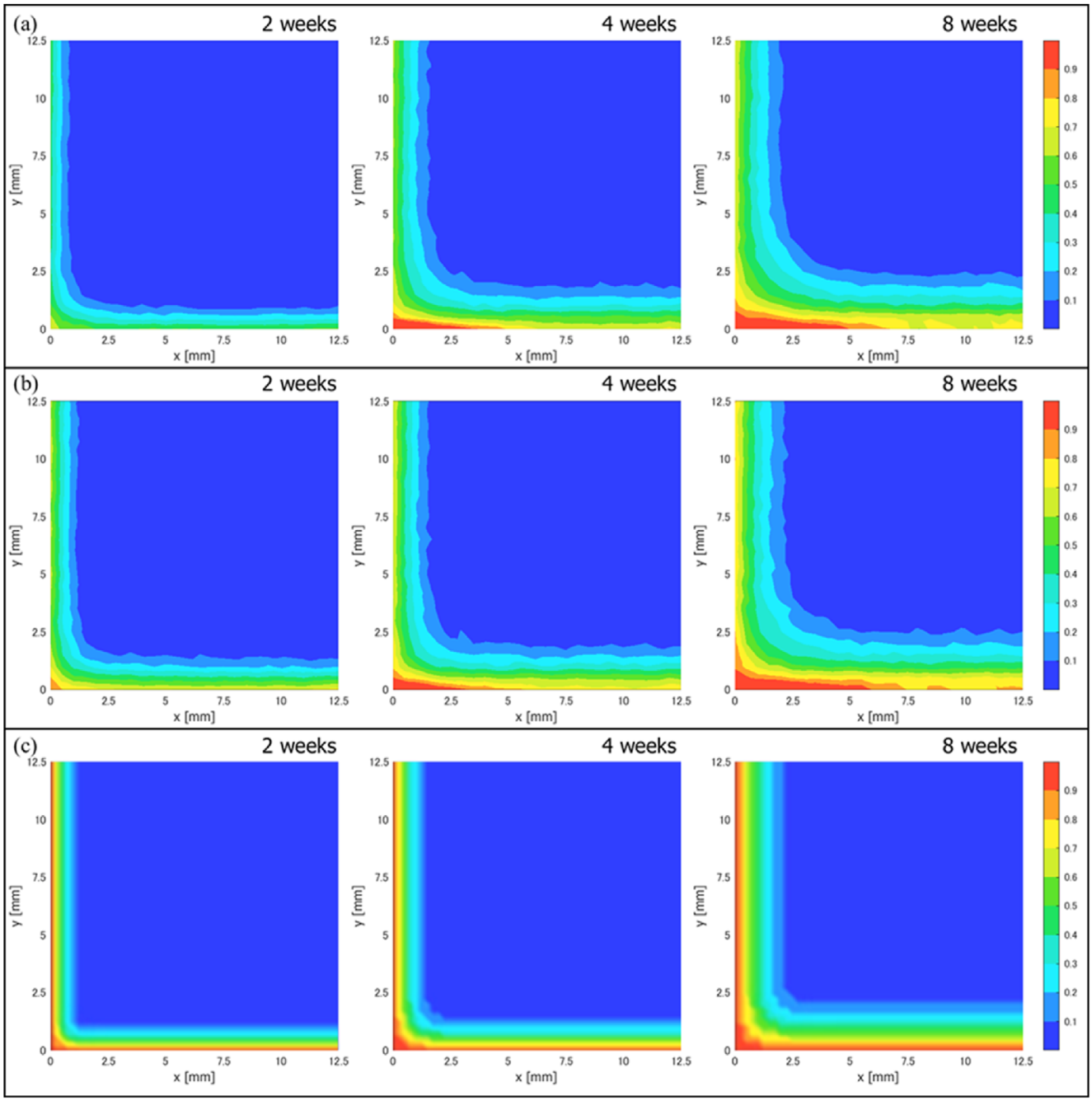

FIGURE 14 Moisture distributions of a closed specimen under immersion at 23°C, determined based on (a) peak intensity of absorbance spectrum, (b) peak intensity of second derivative spectrum, and (c) numerical analysis for 2, 4, and 8 weeks. [Color figure can be viewed at wileyonlinelibrary.com]

At high temperatures, in addition to the diffusion of moisture into the epoxy adhesive, hydrolysis is observed, resulting in decreased crosslink density, increased hydrophilicity, and chemical degradation.[63] Consequently, the observations under long-term immersion at high temperatures may show different trends from those at low temperatures. At 63°C, a change in the peak intensity or weight increment was confirmed (see arrows in Figures 10a, b and 12a), which can be considered as the start of the second stage. That is, the second stage began approximately 1 week after the start of immersion. In addition, the deviation among the peak intensity of the absorbance, that of second derivative spectra, and weight increment increased after 1 week, as shown in Figures 10c, 12b, c. Therefore, prolonged immersion at 63°C cannot be quantitatively assessed due to effects associated with the second stage of diffusion.

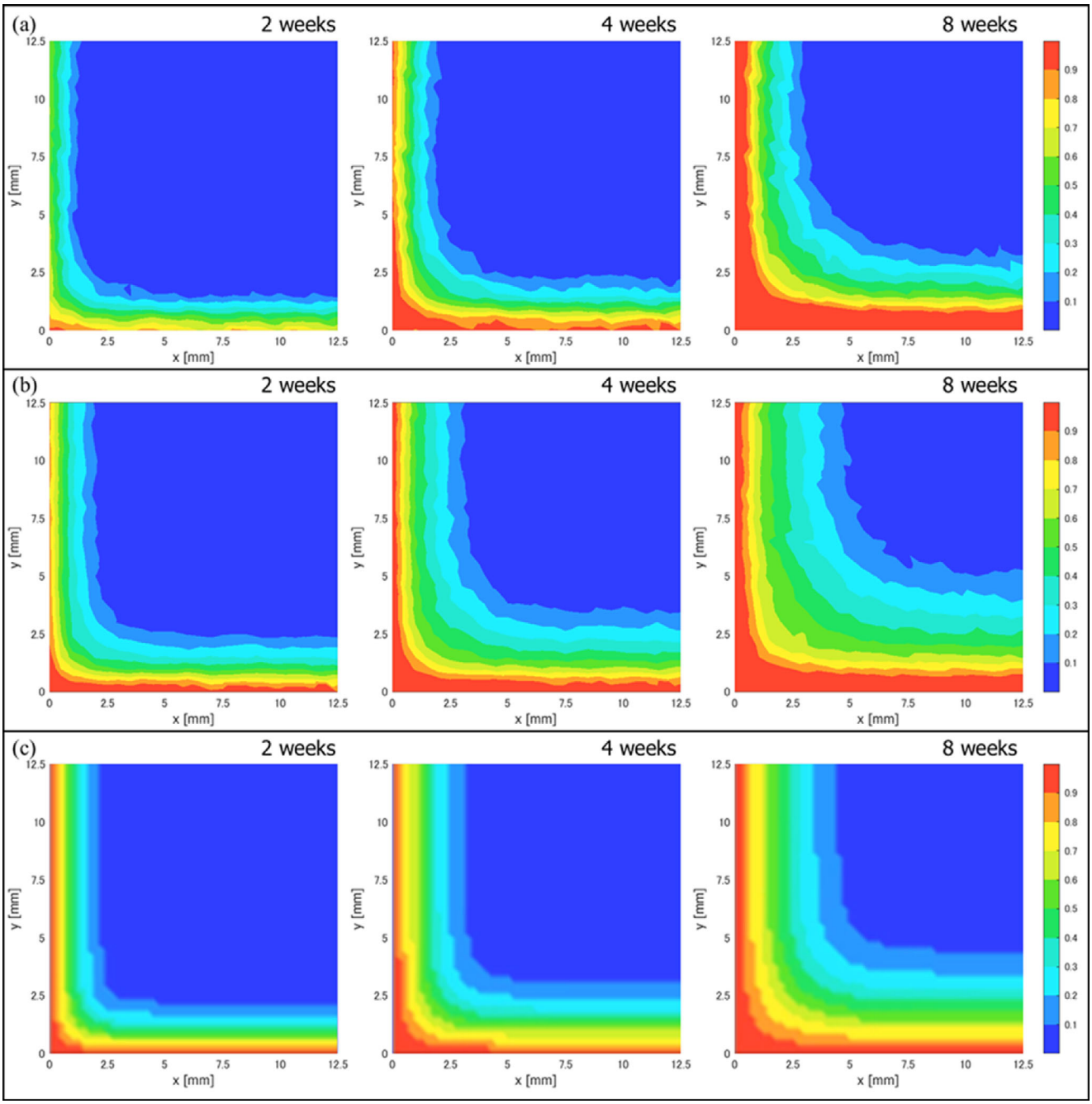

FIGURE 15 Moisture distributions of a closed specimen under immersion at 42°C, determined based on (a) peak intensity of absorbance spectrum, (b) peak intensity of second derivative spectrum, and (c) numerical analysis for 2, 4, and 8 weeks. [Color figure can be viewed at wileyonlinelibrary.com]

To investigate the relationship between the weight increment and peak intensity in greater detail, the peak intensities of the absorption and second derivative spectra and weight increment results were analyzed by normalizing the data with the values at 23°C after 7 days, as shown in Figure 12b, c. Because the measurement times did not match perfectly, the results of the weight increment were linearly interpolated between the data points. By fitting the data for up to 7 days with $y = kx$, the gradient and coefficient of determination were obtained, as shown in Table 2. It was revealed that the peak intensity tended to be slightly larger than the weight increment, especially at 42 and 63°C, but the linearity was maintained. The reverse situation was observed at 63°C after 7 days. In this phase, the weight increment was much larger than the peak intensity. One possible reason might be the change in the vibration spectrum of O—H accompanied by changes in the morphology of the water

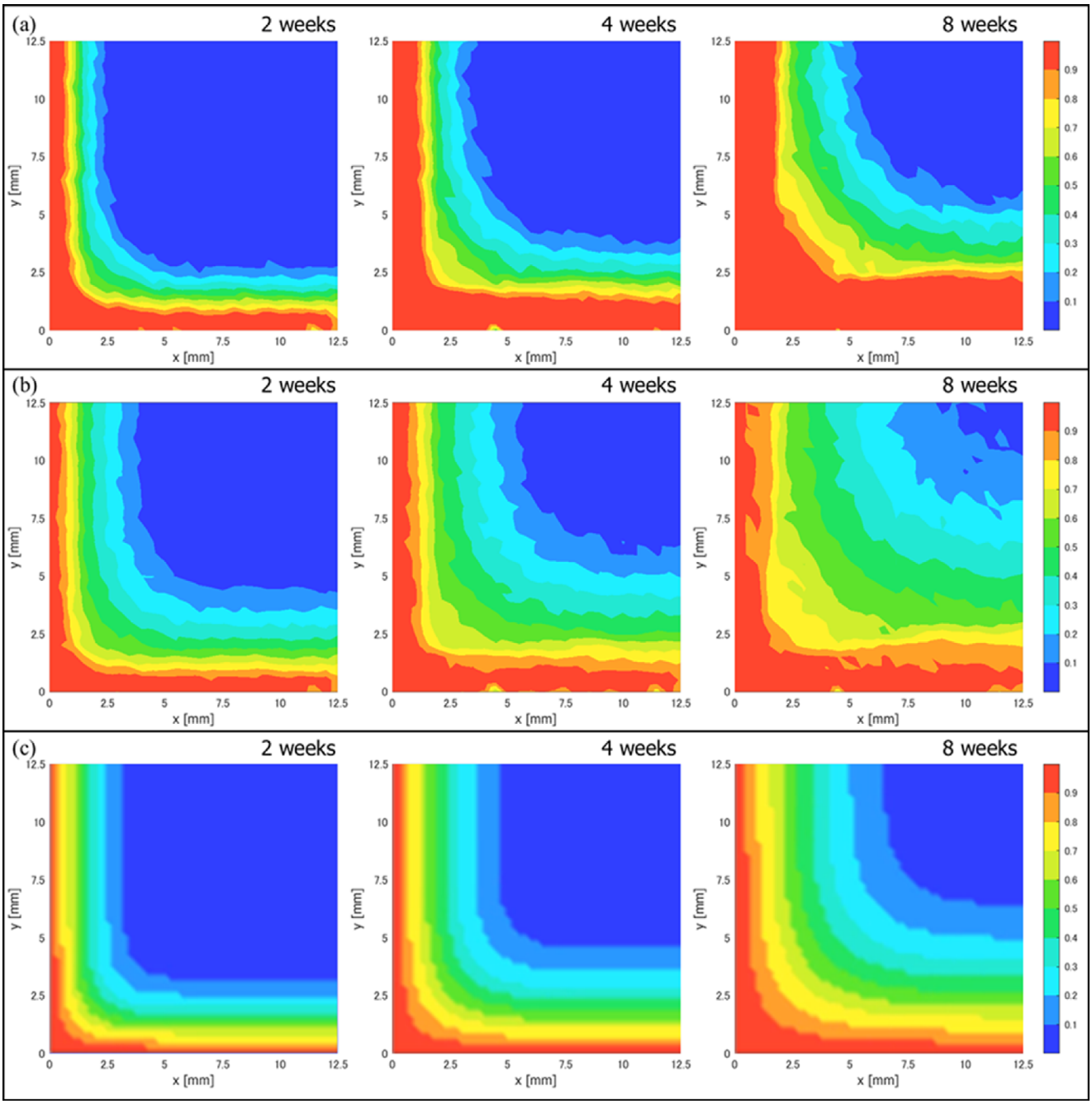

FIGURE 16 Moisture distributions of a closed specimen under immersion at 63°C, determined based on (a) peak intensity of absorbance spectrum, (b) peak intensity of second derivative spectrum, and (c) numerical analysis for 2, 4, and 8 weeks. [Color figure can be viewed at wileyonlinelibrary.com]

molecules, but further investigation is necessary to explain why the absorbance related to H_2O does not increase with increasing mass in the second stage. Here, we can conclude that the peak intensity can indicate the presence of water and can be used to quantitatively evaluate the increase in water content during the first stage of the Fickian diffusion, but only qualitative evaluation is possible during the second stage.

3.2 | Moisture distribution in adhesive layer

Based on the analytical results of the open-faced specimens, the moisture distribution of the closed specimens was measured using the peak intensities of the absorbance and the second derivative spectra. Thermal analysis using the finite element method (FEM) is often employed in the

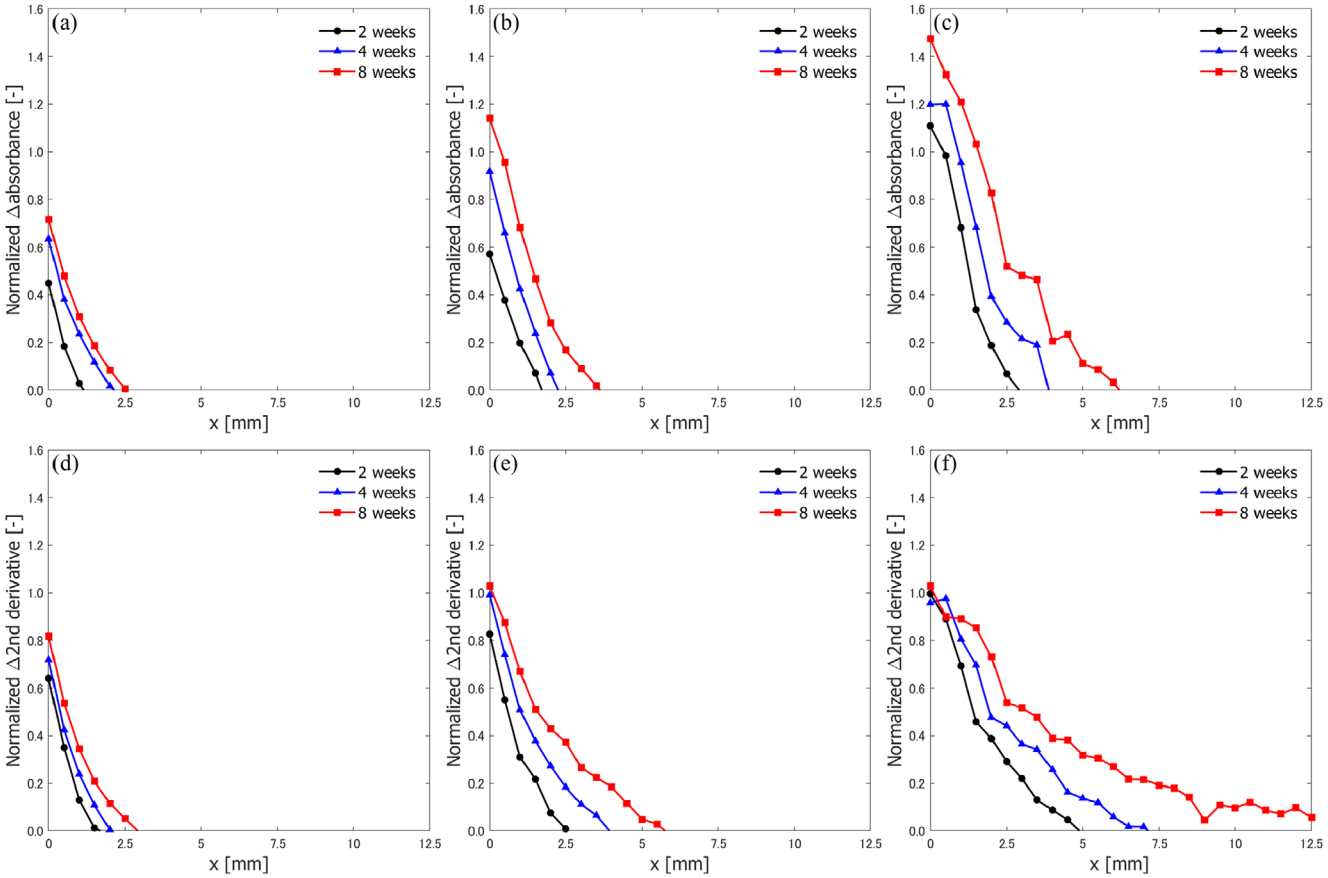

FIGURE 17 Normalized peak intensity profiles of the closed specimens at $y = 12.5$ mm for (a)–(c) the absorbance spectra and (d)–(f) the second derivative spectra at 23, 42, and 63°C, respectively. $x = 0$ mm represents the edge and $x = 12.5$ mm represents the center of the adhesive layer. [Color figure can be viewed at wileyonlinelibrary.com]

simulation of moisture diffusion because the mathematical models are similar. Diffusion coefficients were obtained from the gravimetric test results using Fick's law of diffusion by fitting the early-stage data and were used for 3D analysis using LS-Dyna software. A heat transfer analysis "Mat_thermal_isotropic" was used, and solid elements were employed with a mesh size of 0.125 mm in the longitudinal direction and 0.3 mm in the thickness direction, which is fine enough to evaluate the in-plane distribution. Boundary conditions were defined as saturation of the surface in contact with water and insulation of the interface, such that moisture penetrates only from the outer surface of the adhesive layer, as shown in Figure 13.

The moisture distributions at 23, 42, and 63°C are shown in Figures 14a, 15a, and 16a for the experimental results of the absorbance spectrum, in Figures 14b, 15b, and 16b for the experimental results of the second derivative spectrum, and in Figures 14c, 15c, and 16c for the numerical results, respectively. The peak intensity values were normalized to the maximum value at 23°C for 8 weeks. If little water was absorbed and no peaks were present, peak intensities were considered negligible or negative. Because a negative peak has no physical meaning with respect to water detection, the minimum contour was set below 0.1.

Similar to the results of the open-faced specimen, the peak intensities of the second derivative spectrum tended to be stronger than those of the absorbance spectrum at higher immersion temperatures. However, the changes with respect to the temperature were almost the same. The hotter the water, the greater was the penetration. Figure 17 shows the distribution of moisture absorption for $y = 12.5$ mm (centerline of the specimen). In both methods, the results at 23°C showed a few millimeters of water penetration after 8 weeks, and the penetration distance was longer at higher temperatures.

Compared with the experimentally obtained diffusion maps, the overall trends of the numerical results were consistent, particularly at 23 and 42°C, but a slight difference in the amount of penetration in the corner (left bottom area) was observed. More water soaks into the adhesive layer at the edge than in Fickian diffusion. As the penetration front is always in the initial diffusion condition, the first stage should be strongly related to the

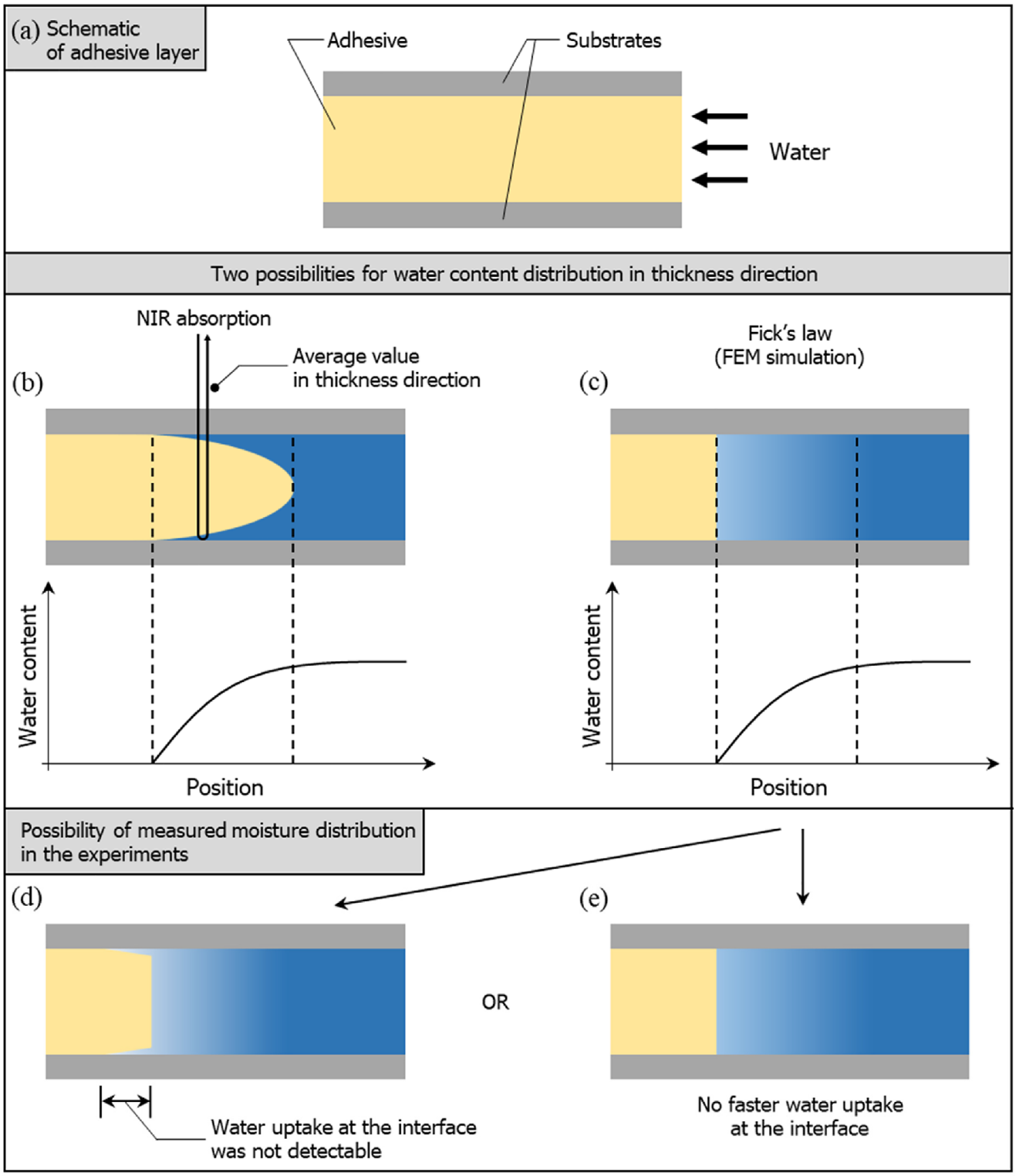

FIGURE 18 The schematic diagram of the water-permeability distribution of the thickness direction of an adhesive layer. (a) Schematic of adhesive layer; (b) the case of water penetration speed near the interface becomes much faster than that of bulk; (c) the case of the FEM calculation using Fick's law of diffusion assumed monotonical penetration in the thickness direction; (d) a posibility that the thickness of the water uptake region near the interface is too thin; (e) the other posibility that no faster water uptake at the interface. [Color figure can be viewed at wileyonlinelibrary.com]

penetration distance. Therefore, the numerical calculations based on Fick's law of diffusion by using the diffusion coefficients obtained from the early-stage data of diffusion are considered to agree well with the experimental results. Conversely, in the case of long-term immersion at 63°C, a large difference was observed between the experimentally

measured distribution map and the FEM calculated distribution map. At high-temperature immersion, various chemical and physical changes are believed to have occurred to the epoxy resin in addition to water absorption, and so it is difficult to accurately analyze the moisture content based on only the observations of the spectral changes. Therefore, the NIRS can only be used for relatively low-temperature immersion for quantitative analysis of water content. However, without actual observations, verification of the numerical results is impossible, and the proposed experimental scanning method has great potential for examining the accuracy of numerical diffusion analysis.

Figure 18 shows the schematics of moisture penetration in the thickness direction in the adhesive layer. In some experiments, the coefficient of diffusion of the adhesive layer was much larger than that of bulk and it was suggested that water penetration speed near the interface becomes much faster,[35] as shown in Figure 18b. Conversely, in the FEM calculation using Fick's law of diffusion, monotonically penetration in the thickness direction is assumed, as shown in Figure 18c. When NIR absorption values are used to evaluate moisture content, it is not possible to discuss how the moisture is distributed in the thickness direction because only the average values in the thickness direction are obtained. However, no significant difference was found between the FEM and experimental results in this study. Therefore, it was considered that the water penetration was close to the case shown in Figure 18c. On the other hand, there still remains a possibility that the diffusion near the interface is faster because the water cannot be detected by the NIRS method if the thickness of the water-penetrated region near the interface is too thin (Figure 18d). Therefore, it cannot be determined whether the penetration speeds of the bulk and adhesive layer are different, but even if they are different, it can be concluded that the total moisture content of the adhesive layer does not deviate significantly from the value calculated using the coefficient of diffusion of bulk. According to the model in ref [35], the penetration rate near the interface varies with wettability. Therefore, further investigation such as changing the surface wettability of the substrates may increase a deeper understanding of water penetration in the adhesive layer.

4 | CONCLUSIONS

We performed the spectral analysis of moisture penetration into an epoxy adhesive and observed the moisture diffusion in the adhesive layer by using a fiber-type NIRS instrument. First, the change in the NIR spectrum owing to the water content of the epoxy was investigated. With increasing water content, a peak appeared in the absorbance spectrum at approximately 1900–1950 nm. It was confirmed that the peak intensities of the absorbance spectra were correlated with those of the second derivative spectra. In addition, the peak intensity variation showed similar trends as the weight increment, particularly at the initial diffusion stage. Next, the distribution of moisture diffusion in the adhesive layer was investigated. Specially prepared adhesively bonded joints prepared using a quartz glass plate were used, and the peak intensities of the NIR spectrum were measured via surface scanning without destroying the joints. In the case of the adhesive used, moisture penetrated approximately 2.5 mm after 8 weeks of immersion at 23°C. For comparison, FEM analysis using the diffusion coefficients of the initial stage of diffusion was also conducted. The measured diffusion map showed good agreement with the numerical results, particularly at lower immersion temperatures. Therefore, we succeeded in developing a moisture distribution observation method for the adhesive layer using NIRS, and clarified that the FEM analysis method using Fick's law of diffusion can accurately estimate the penetration distance. Although the reliability of the quantitative assessment of high-temperature immersion remains debatable, this study established the usefulness of the NIRS method in understanding this phenomenon. Many problems related to the effects of water on adhesive joints remain. The effect of surface conditions or others on the moisture penetration speed can be clarified by using this technique. Therefore, it is expected that this method will advance the elucidation of the associated phenomena.

AUTHOR CONTRIBUTIONS

Jin-Woo Han: Data curation (lead); formal analysis (lead); investigation (lead); methodology (lead); software (lead); validation (lead); visualization (lead); writing – original draft (lead). **Yu Sekiguchi:** Data curation (supporting); project administration (supporting); supervision (lead); validation (supporting); writing – review and editing (lead). **Kazumasa Shimamoto:** Data curation (supporting); methodology (supporting); validation (supporting); writing – review and editing (supporting). **Haruhisa Akiyama:** Conceptualization (supporting); methodology (supporting); writing – review and editing (supporting). **Chiaki Sato:** Conceptualization (lead); project administration (lead); supervision (lead).

ACKNOWLEDGMENTS

This work is based on the results obtained from a project commissioned by the New Energy and Industrial Technology Development Organization (NEDO). We would like to thank all the project members for their contributions. We are thankful to Cemedine Co., Ltd. for supplying the materials.

FUNDING INFORMATION

This research was funded by New Energy and Industrial Technology Development Organization (NEDO) under Project Number JPNP14014.

CONFLICT OF INTEREST STATEMENT

The authors declare no conflicts of interest.

DATA AVAILABILITY STATEMENT

The data that support the findings of this study are available from the corresponding author upon reasonable request.

ORCID

Jin-Woo Han https://orcid.org/0000-0001-7703-9120

REFERENCES

[1] M. D. Banea, L. F. M. da Silva, *Proc. Inst. Mech. Eng. L: J. Mater. Des. Appl.* **2010**, *224*, 51.
[2] F. Cavezza, M. Boehm, H. Terryn, T. Hauffman, *Metals* **2020**, *10*, 730.
[3] H. Naji Mehr, M. Shariati, P. Zamani, L. F. M. da Silva, D. G. Moghadam, *J. Appl. Polym. Sci.* **2021**, *139*, 52069.
[4] P. Zamani, A. Jaamialahmadi, L. F. M. da Silva, *Int. J. Adhes. Adhes.* **2023**, *122*, 103338.
[5] M. Moazzami, M. R. Ayatollahi, A. Akhavan-Safar, L. F. M. da Silva, *Polym. Test.* **2020**, *91*, 106789.
[6] J. A. da Costa, A. Akhaban-Safar, E. A. S. Marques, R. J. C. Carbas, L. F. M. da Silva, *Int. J. Fatigue* **2022**, *161*, 106939.
[7] M. Costa, G. Viana, L. F. M. da Silva, R. D. S. G. Campilho, *Proc. Inst. Mech. Eng. L: J. Mater. Des. Appl.* **2018**, *232*, 733.
[8] F. M. G. Ramírez, M. F. S. F. de Moura, R. D. F. Moreira, F. G. A. Silva, *Fatigue Fract. Eng. Mater. Struct.* **2020**, *43*, 1307.
[9] H. Khoramishad, H. Bayati, D. Kordzangeneh, *J. Adhes.* **2022**, *98*, 507.
[10] W.-L. Mu, Q.-H. Xu, J.-X. Na, H. Wang, W. Tan, D.-F. Li, *J. Adhes.* **2022**, *98*, 1358.
[11] C. S. P. Borges, E. A. S. Marques, R. J. C. Carbas, C. Ueffing, P. Weißgraeber, L. F. M. da Silva, *Proc. Inst. Mech. Eng. C: J. Mech. Eng. Sci.* **2021**, *235*, 527.
[12] H.-S. Kim, J. Huh, J. Ryu, *J. Phys. D: Appl. Phys.* **2011**, *44*, 034007.
[13] K. Shimamoto, S. Batorova, K. Houjou, H. Akiyama, C. Sato, *J. Adhes.* **2021**, *97*, 1255.
[14] K. Shimamoto, S. Batorova, K. Houjou, H. Akiyama, C. Sato, *J. Adhes*. **2021**, *97*, 1388.
[15] R. A. A. Lima, F. Migliavacca, L. M. Martulli, M. Carboni, A. Bernasconi, *Theor. Appl. Fract. Mech.* **2022**, *121*, 103501.
[16] A. Bernasconi, L. M. Martulli, M. Carboni, *Int. J. Fatigue* **2022**, *154*, 106526.
[17] F. Sun, R. Zhang, B. R. K. Blackman, *Int. J. Solids Struct.* **2021**, *217-218*, 60.
[18] K. Kamiyama, M. Mikuni, T. Matsumoto, *Int. J. Adhes. Adhes.* **2018**, *83*, 76.
[19] N. Terasaki, Y. Fujio, Y. Sakata, S. Horiuchi, H. Akiyama, *J. Adhes.* **2018**, *94*, 867.
[20] X. Jiang, H. Kolstein, F. Bijlaard, X. Qiang, *Compos. A Appl. Sci. Manuf.* **2014**, *57*, 49.
[21] Y. Pan, G. Xian, M. A. G. Silva, *Constr. Build. Mater.* **2015**, *101*, 326.
[22] V. B. Mora, M. Mieloszyk, W. Ostachowicz, *Mech. Syst. Signal Process.* **2018**, *99*, 534.
[23] S. Sugiman, S. Salman, P. D. Setyawan, S. Sulardjaka, *IOP Conf. Ser. Mater. Sci. Eng.* **2019**, *532*, 012007.
[24] I. A. Ashcroft, A. D. Crocombe, in *Design of adhesive joints under humid conditions. Advanced Structured Materials* (Eds: L. F. M. da Silva, C. Sato), Springer Berlin, Heidelberg, Germany **2013**.
[25] X. Han, A. D. Crocombe, S. N. R. Anwar, P. Hu, *Int. J. Adhes. Adhes.* **2014**, *55*, 1.
[26] S. Liu, X. Cheng, Q. Zhang, J. Zhang, J. Bao, X. Guo, *Compos. B Eng.* **2016**, *91*, 431.
[27] A. R. Zaeri, H. S. Googarchin, *Fatigue Fract. Eng. Mater. Struct.* **2019**, *42*, 929.
[28] S. Sugiman, P. D. Setyawan, S. Salman, H. Ahmad, *Compos. B Eng.* **2019**, *173*, 106977.
[29] X. Han, G. Akhmet, P. Hu, W. Hou, Y. Baubekov, M. Akhmetov, *Compos. Struct.* **2020**, *241*, 112131.
[30] G. Viana, R. J. C. Carbas, M. Costa, M. D. Banea, L. F. M. da Silva, *Proc. Inst. Mech. Eng. C J. Mech. Eng. Sci.* **2021**, *235*, 560.
[31] I. Katsivalis, S. Feih, *Glass Struct. Eng.* **2022**, *7*, 381.
[32] Y. Chao, J. Ma, Z. Chen, Y. Zhang, P. Yang, S. Wang, L. Wang, X. Han, Y. Liu, C. Wu, *J. Adhes.* **2022**, *98*, 553.
[33] W. Li, X. Shao, L. Li, G. Zheng, *J. Adhes.* **2022**, *98*, 2446.
[34] S. Fevery, H. Hallez, D. Vandepitte, S. Debruyne, *Proc. Inst. Mech. Eng. E: J. Process Mech. Eng.* **2020**, *234*, 477.
[35] M. P. Zanni-Deffarges, M. E. R. Shanahan, *Int. J. Adhes. Adhes.* **1995**, *15*, 137.
[36] M. Schneider, U. Gierth, L. Simunkova, P. Gierth, L. Rebenklau, *Mater. Corros.* **2020**, *71*, 1832.
[37] K. Wapner, G. Grundmeier, *Int. J. Adhes. Adhes.* **2004**, *24*, 193.
[38] K. Wapner, M. Stratmann, G. Grundmeier, *Electrochim. Acta* **2006**, *51*, 3303.
[39] E. Siryabe, M. Rénier, A. Meziane, J. Galy, M. Castaings, *Ultrasonics* **2017**, *79*, 34.
[40] B. Yılmaz, E. Jasiūnienė, *Int. J. Adhes. Adhes.* **2020**, *102*, 102675.
[41] M. Clavaud, Y. Roggo, K. Dégardin, P.-Y. Sacré, P. Hubert, E. Ziemons, *J. Pharm. Biomed. Anal.* **2016**, *131*, 380.
[42] M. T. J. Benito, C. B. Ojeda, F. S. Rojas, *Appl. Spectrosc. Rev.* **2008**, *43*, 452.
[43] R. Moscetti, F. Raponi, S. Ferri, A. Colantoni, D. Monarca, R. Massantini, *J. Food Eng.* **2018**, *222*, 139.
[44] W. Camacho, A. Vallés-Lluch, A. Ribes-Freus, S. Karlsson, *J. Appl. Polym. Sci.* **2003**, *87*, 2165.
[45] S. Beguš, G. Beguš, J. Drnovšek, D. Hudoklin, *Sens. Actuators A: Phys.* **2015**, *211*, 53.
[46] M. Manley, *Chem. Soc. Rev.* **2014**, *43*, 8200.
[47] Y. Wei, F. Wu, J. Xu, J. Sha, Z. Zhao, Y. He, X. Li, *J. Food Eng.* **2019**, *248*, 89.
[48] O. Daikos, T. Scherzer, *Prog. Org. Coat.* **2022**, *163*, 106610.
[49] S. Kumar, S. Kansal, M. H. Alkinani, A. Elaraby, S. Garg, S. Natarajan, V. Sharma, *Electron.* **2022**, *11*, 2611.
[50] B. Buttingsrud, B. Alsberg, *Chemom. Intell. Lab. Syst.* **2006**, *84*, 62.
[51] K. B. Beć, J. Grabska, C. W. Huck, *Chem. Eur. J.* **2021**, *27*, 1514.
[52] K. B. Whetsel, *Appl. Spectrosc. Rev.* **1968**, *2*, 1.
[53] Y. Li, H.-W. Chen, X.-Y. Xia, G.-Y. Ma, H.-P. Tan, *Int. Commun. Heat Mass Transf.* **2021**, *125*, 105290.

[54] T. Mohammadi-Moghaddam, S. M. A. Razavi, A. Sazgarnia, M. Taghizadeh, *J. Food Meas. Charact.* **2018**, *12*, 346.
[55] J. Torniainen, I. O. Afara, M. Prakash, J. K. Sarin, L. Stenroth, J. Töyräs, *Anal. Chim. Acta* **2020**, *1108*, 1.
[56] B. Hofko, M. Z. Alavi, H. Grothe, D. Jones, J. Harvey, *Mater. Struct.* **2017**, *50*, 187.
[57] A. A. Christy, *Vib. Spectrosc.* **2010**, *54*, 42.
[58] J. S. Panero, H. E. B. da Silva, P. S. Panero, O. J. Smiderie, F. S. Panero, F. S. E. D. V. Faria, A. F. R. Rodriguez, *J. Agric. Sci.* **2018**, *10*, 351.
[59] J. Rantanen, E. Räsänen, J. Tenhunen, M. Känsäkoski, J.-P. Mannermaa, J. Yliruusia, *Eur. J. Pharm. Biopharm.* **2000**, *50*, 271.
[60] Å. Rinnan, F. V. D. Berg, S. B. Engelsen, *TrAC, Trends Anal. Chem.* **2009**, *28*, 1201.
[61] M. D. Placette, X. Fan, J.-H. Zhao, D. Edwards, *Microelectron. Reliab.* **2012**, *52*, 1401.
[62] C. Gillet, F. Tamssaouet, B. Hassoune-Rhabbour, T. Tchalla, V. Nassiet, *Polymer* **2022**, *14*, 2832.
[63] G. Capiel, J. Uicich, D. Fasce, P. E. Montemartini, *Polym. Degrad. Stab.* **2018**, *153*, 165.

How to cite this article: J.-W. Han, Y. Sekiguchi, K. Shimamoto, H. Akiyama, C. Sato, *J. Appl. Polym. Sci.* **2023**, *140*(25), e53982. https://doi.org/10.1002/app.53982